DOI: 10.1039/C6RA17516C

RSC Advances

PAPER

View Article Online
View Journal | View Issue

Cite this: *RSC Adv.*, 2016, **6**, 84769

Fabrication of interdigitated micro-supercapacitor devices by direct laser writing onto ultra-thin, flexible and free-standing graphite oxide films

Rajesh Kumar,*[a] Raluca Savu,[a] Ednan Joanni,[b] Alfredo R. Vaz,[a] Mara A. Canesqui,[a] Rajesh K. Singh,[c] Ronaldo A. Timm,[d] Lauro T. Kubota[d] and Stanislav A. Moshkalev*[a]

Received 8th July 2016
Accepted 30th August 2016

DOI: 10.1039/c6ra17516c

www.rsc.org/advances

In this work we present graphene-based in-plane flexible interdigitated micro-supercapacitor devices fabricated through direct laser writing onto ultra-thin graphite oxide (GO) films. The fabrication route is simple, fast, additive-free, mask-free and cost effective. This involves direct micro-writing of reduced graphene oxide (rGO) by a pulsed UV laser on a very small area (1.14 cm^2). The fabricated micro-supercapacitor contains nineteen pairs of rGO electrodes separated by the unreduced portion of the GO film. The single laser patterned rGO electrode presents low resistivity, while the unpatterned portion is non-conducting. Under the optimized laser parameters the 2.2 μm ultra-thin GO films were completely and uniformly reduced. The electrochemical measurements showed that the micro-supercapacitor, packed in a glass cavity, and in the presence of a liquid electrolyte have a capacitance nearly 288% higher (288.7 mF cm^{-3}) compared to the as-fabricated device (0.36 mF cm^{-3}). The as-fabricated micro-supercapacitor without electrolyte also shows some capacitance due to the presence of free ions in the unreduced portion of GO which plays a crucial role. Furthermore, the cycling stability of the as-fabricated micro-supercapacitor is robust, with not much performance degradation for more that 5000 cycles.

1. Introduction

Among the devices developed for better energy harvesting and storage, electrochemical supercapacitors have been extensively studied and proved to be an excellent option for energy storage.[1–3] Electrochemical supercapacitors have attracted vast attention due to higher power density and longer life cycle compared to batteries, and higher energy density than conventional dielectric capacitors.[4] The development of high performance electrical energy storage systems has been a major concern for industries as well as societies for the last few decades.[5–7] The supercapacitors store and release energy based on either the accumulation of charges at the interface between electrodes and electrolyte (electrical double layer capacitors – EDLC) or on fast and reversible faradic redox reactions (pseudocapacitors), or both, mainly depends on the nature of the active material used.[8] Recently, intensive efforts are made for fabricating high performance supercapacitors having elevated energy and power density with long-time cycle stability.[8–12]

Nowadays, the recent technological trend of using flexible/wearable electronic devices has increased the need of micro-power sources and small-scale energy storage devices.[13–15] Flexible micro-electronic systems, including rolled-up, bendable displays, wearable multimedia devices, *etc.*, require extremely thin and flexible power supplies.[16–20] Thus, flexible electrochemical supercapacitors have been considered as one of the most promising contenders compared with conventional energy storage devices due to their flexibility, lightweight, and low-cost. Development of new electrochemical supercapacitors, also known as micro-supercapacitors, aroused special attention due to their possible integration into miniaturized portable electronic devices such as micro-electromechanical systems or micro-robots, and act as micro power sources for energy harvesting.[21–25]

Recently, different research groups have made considerable contributions to the fabrication of micro-supercapacitors and other devices by carbonization of polymer sheets by laser,[6,21,26,27] 3D nanofabrication of different nanostructures on various substrates by direct laser writing[28–32] and printing through lithographic processes.[33–36] These methods suffer from various disadvantages like lack of fine patterning, constraints on the substrate or fabrication speed. Also, in the above contributions, the laser technique used is

[a]*Centre for Semiconductor Components and Nanotechnology (CCS Nano), University of Campinas (UNICAMP), Campinas, 13083-870, Brazil. E-mail: rajeshbhu1@gmail.com; stanisla@ccs.unicamp.br*

[b]*Centre for Information Technology Renato Archer (CTI), Campinas, 13069-901, Brazil*

[c]*School of Physical and Material Sciences, Central University of Himanchal Pradesh (CUHP), Kangra, Dharamshala, HP-176215, India*

[d]*Department of Analytical Chemistry, Institute of Chemistry, University of Campinas (UNICAMP), Campinas, 13084-971, Brazil*

simple and consistent in delivering the concentrated thermal energy in the precise direction for diverse micro patterning. Instead of using polymer over different substrates, graphite oxide can be used directly and converted into graphene, which has unique properties of large surface area, excellent stability, high Young's modulus and high thermal/electric conductivity.[37–40] There has been an ongoing trend to employ graphene materials to replace the usage of polymer sheets on various substrates for energy conversion and energy storage devices, to incur lower costs and environmental benignity of these materials. Lasers are applied for the fabrication of micro-supercapacitors, wherein the role of the laser has been to locally reduce graphite oxide and induce morphological changes leading to porous structures to enhance the accessibility to ions.[41–43] The direct laser writing technique has been proposed and appears to be one of the promising approaches for micro devices fabrication. Compared with the conventional printing and lithographic approaches, the direct laser writing approach provides higher flexibility for arbitrary graphene patterning *via* non-contact and mask-free fabrication processes, which highly reduces the manufacturing costs. Several groups fabricated micro-supercapacitors using different sources of carbon and distinct techniques, like laser irradiation and UV patterning. Ajayan's group[43] reported fabrication of micro-supercapacitors on thick hydrated GO film (22 μm) by reducing the GO film into interdigitated electrode through the use of CO_2 laser. Tour's group[27] used thick polyimide films (0.005″) for fabrication of micro-supercapacitors by transforming into porous graphene also through CO_2 laser system. In turn, Mullen's group[44] reported fabrication of micro-supercapacitors using lithography involving several processing steps like masking, pattering and etching of graphene oxide surface and fabrication of the interdigitated patterns through the deposition of gold.

In this work, we demonstrate an improved method for one-step fabrication of micro-supercapacitors by facile direct laser writing induced reduction of ultra-thin and free-standing GO film. Also, the direct laser writing seems to have vast potential applications for quick and scalable synthesis of impurity-free graphene patterns on GO film for interdigitated electrodes. More importantly, direct laser writing achieves single-step micro-supercapacitor fabrication of the graphene electrode patterns by combining both graphene reduction and patterning steps, resulting in a significantly enhanced efficiency.

2. Experimental section

2.1 Materials

Potassium permanganate ($KMnO_4$, 98%), hydrochloric acid (HCl, 37%) and sulfuric acid (H_2SO_4 reagent grade, 95.0–98.0%) were acquired from Synth (Sao Paulo-Brazil). Graphite flakes (Graflake 99580, 99.50% purity) were provided by Nacional de Grafite, Brazil. All other chemicals used were of analytical grade or better quality and used without further purification. Aqueous solutions were prepared with ultrapure water (>18 MΩ cm) obtained from a Milli-Q Plus system (Millipore).

2.2 Synthesis of graphite oxide (GO) solution

Graphite oxide was synthesized employing modified Hummer's method.[45] Briefly, 1.0 g of graphite flakes were mixed into a rounded bottom flask containing 100.0 ml of 98.0% H_2SO_4 under stirring and with controlled temperature (<40 °C). Afterwards, 2 g of $KMnO_4$ was slowly added to the reaction, generating a characteristic green color attributed to the oxidizing agent, dimanganese-heptoxide (Mn_2O_7).[46,47] When the oxidation process was over, 250 ml of ultra-pure water (in ice form) was added and, subsequently, poured 4.0 ml of 30% H_2O_2 to deplete residual $KMnO_4$ present during preparation. The resulting solution was centrifuged and washed with deionized water and 5% HCl (v/v) solution. After this, several washes using deionized water were made to remove acidic species. Finally, GO dispersed in water was purified by dialysis using cellulose tubular membrane for one week for removal of remaining salt impurities. The resulting suspension of GO having concentration of 1.7 mg ml^{-1} was stored in this form.

2.3 Preparation of ultra-thin GO free standing thin film

The above prepared GO solution was vacuum filtered through a 47 mm diameter Millipore (type HA) membrane with a pore size of 0.45 μm. For a typical free standing and ultra-thin GO film, 50 ml of the dispersion was poured into a vacuum filtration setup and filtered under low vacuum. The GO thin film was peeled off from the membrane filter after complete drying in air. The resulting peeled-off film is free-standing and possesses flexible nature, being 35 mm in diameter and ~2.2 μm thick, and was used to fabricate the final micro-supercapacitor device employing direct laser writing.

2.4 Local reduction of GO film by laser writing

Reduced GO regions were directly fabricated through a laser-treatment system composed of a computer controlled movable *x*, *y* linear stages with a 40 nm minimum step, *z* focus adjustment and a diode-pumped solid-state laser (DPSSL). The GO thin film was placed on the *xy* controlled table under the stationary laser source, and the interdigitated electrodes were drawn through direct laser reduction of the GO film in air using a Nd:YVO_4 pulsed laser ($\lambda = 355$ nm), with pulse duration of 20 ns, 20 μm minimum spot size, 20 W maximum power using a custom-built software for pattern design and movement control.

The effects of different laser treatment conditions on the electrical conductivity of the rGO films were systematically investigated. Several rGO linear trajectory paths were drawn through direct laser writing on the GO films with different laser scanning speeds (at fixed laser power of 244 mW). The manifestation of dark rGO lines on the brown GO film after the laser scanning initially confirmed the reduction of GO.[29] In order to investigate the effect of the laser scan speed, patterning was prepared using speeds ranging from 0.5 to 5 mm s^{-1}, with an increment step of 0.5 mm s^{-1}. The effect of laser power, at constant speed, on the electrodes pattern quality was also tested. Several rGO electrode lines were drawn on GO film with different laser power (130, 164, 218, 244, 310, 344 and 376 mW) at a fixed laser scan speed of 2.5 mm s^{-1}.

2.5 Fabrication of micro-supercapacitors

After optimization of the various experimental parameters for direct laser writing, flexible micro-supercapacitors were designed and fabricated onto thin, semi-transparent GO films. The micro-supercapacitor were fabricated with an area of 1.14 cm^2 (19 mm length and 6 mm width) on 2.2 mm thin GO films by direct laser writing. Each electrode consists of 5 mm length, 100 μm width (reduced) with uniform linear reduction with spacing of 400 μm (unreduced) between electrodes. The as-fabricated micro-supercapacitor had 19 parallel pairs of rGO electrodes, with equal number of conjugated electrodes on each side. The device contains two rGO contact pads 2.5 × 2.5 mm^2 for electrochemical measurements.

2.6 Sample characterization

The 2.2 μm thick freestanding GO films and reduced portions were characterized using scanning electron microscopy, Raman spectroscopy, optical microscopy and current–potential (*I–V*) measurements. Scanning electron microscopic images were taken on a FEG microscope from FEI company (Dual Beam FIB/FEG model Nova 200) using an electron beam current ranges from 0.4–1.6 nA and 5–10 kV energy. In order to avoid charging of the insulating GO film, as the one shown in Fig. 1b, a fine metallic contact was clamped onto one corner of the sample. Raman measurements were carried out using a spectrometer with 473 nm laser (NT-MDT NTEGRA Spectra). Optical microscopic studies were carried out on Olympus MX51-F Microscope under reflectance mode. GO and rGO sheet resistance measurements and the *I–V* measurements were performed using a 2636A source-meter (Keithley Instruments, Inc.) by applying biases from −1 V to 1 V.

2.7 Electrochemical measurements of flexible micro-supercapacitor

All the electrochemical measurements were performed using a two-electrode configuration as it is more relevant for the concerned practical applications. Areal and volumetric specific capacitances are measured and reported as they are more relevant than gravimetric capacitance for micro-scale applications. Also, thin micro-supercapacitors are used, the gravimetric capacitance may not be accurate due to the small amount of material used as sample.[48] Hence, we have calculated the areal and volumetric capacitance of the micro-supercapacitor devices by considering the total area and volume of the material between the electrodes. All measurements were performed on an AUTOLAB modular electrochemical system (ECO Chemie, Ultrecht, Netherlands) equipped with a STAT 12 module, driven by Nova (v1.10) software and a computer for data storage and processing. AC impedance spectroscopy was used to probe the frequency response of the device. The CV curves of flexible micro-supercapacitor devices were measured between 0 and 1.2 V with various scan rates in the range of 0.3–1.0 V s^{-1}. The measurements were carried out in a 0.1 M Na_2SO_4 aqueous electrolyte solution at room temperature.

Standard cyclic voltammetry (CV) measurements were performed in order to thoroughly characterize the as fabricated micro-supercapacitors. The interdigitated micro-supercapacitor devices were subjected to cyclic voltage sweeps at various scan rates from 0.3 to 1.0 V s^{-1} (0.1 V s^{-1} step) without electrolyte (CI) and in open air. We observed that the electrolyte/water solution placed over the micro capacitors was evaporating during long-term tests, possibly affecting the results, we used four different conditions for comparative testing: (a) electrochemical measurements of as-made patterns without any electrolyte (CI); (b) measurements with 0.1 M Na_2SO_4 aqueous electrolyte solution (CII); (c) devices placed in a glass cavity, with the cavity being filled with electrolyte and covered with top glass plate to prevent electrolyte evaporation during long time electrochemical measurements (CIII) and (d) the micro-supercapacitor in a cavity after removing the electrolyte from glass cavity (completely dry environment without electrolyte) (CIV). For the CII tests, we poured the electrolyte on the interdigitated electrodes of the micro-supercapacitor in air. For CIII and CIV tests, we used a glass cavity of lateral size corresponding to the dimensions of the micro-supercapacitor and a height of 2 mm.

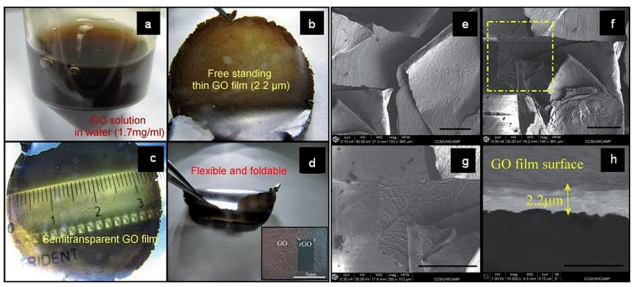

Fig. 1 Optical images of: (a) GO solution (1.7 mg ml^{-1} in water) used for obtaining (b) free-standing, (c) semi-transparent, (d) flexible and foldable ultra-thin GO film used for fabrication of micro-supercapacitor device. Inset shows the color changes from brown to black due to reduction after direct laser writing on GO film. Surface and cross-sectional SEM micrographs of as synthesized ultra-thin GO film: (e, f) lower and (g) higher magnification (yellow square in f) of its surface and (h) cross-sectional view showing film thickness (scale bar e–g = 200 μm and h = 5 μm).

3. Result and discussion

3.1 Morphological characterization by microscopy

Fig. 1a shows the optical image of GO suspension with a concentration of 1.7 mg ml^{-1} GO powder in H_2O and its conversion into free standing and ultra-thin GO film (paper) through vacuum filtration at room temperature (Fig. 1b and c). The as synthesized GO film is very thin (~2.2 μm thickness; diameter of 35 mm), of semi-transparent nature, flexible and foldable (Fig. 1c and d). The free-standing film shows a high optical transparency (Fig. 1c), and the inset in Fig. 1d shows that the GO thin film can be locally converted to reduced graphene oxide (rGO) through direct focused laser irradiation. The brownish color of GO completely changes to dark black (rGO) after laser irradiation, the reduction process being later confirmed by further morphological and electrical characterizations.

Fig. 1e–h shows SEM micrographs of as synthesized free-standing GO thin film prepared from the GO solution (Fig. 1a) at different magnifications. The as synthesized GO film consists of many compactly packed plane thin sheets with lateral dimensions of 200–500 μm and contains wrinkles on the surface, probably due to the influence of attached functional groups on the surfaces. The cross-sectional view shows the thickness of 2.2 μm for as synthesized GO thin film (Fig. 1h).

3.2 Effect of direct laser writing: electrode width and degree of reduction of GO film

Fig. 2 shows the optical micrographs of locally processed GO surfaces at different laser scan speed and laser power. The laser scanned regions presume a darker coloration and could be clearly distinguished from the unmodified GO film. Fig. 2a–f show clear morphological changes for different laser scan speeds. At lower laser scan speeds ($\leq$1 mm s^{-1}), strong ablation of GO film occurs resulting in partial or complete removal of the GO film instead of its reduction into linear rGO patterns. Above 1.5 mm s^{-1} laser scan speed, visible dark electrode patterns are seen on the GO film. From 1.5 to 5 mm s^{-1}, the width of the dark lines decreases continuously (Fig. 2b–f), and, in general, the lower the laser scan speed, the better is the contrast between processed and non processed areas. Higher laser scan speed as well as lower seems not to be favorable for the complete reduction of GO films. At high speeds GO films are unable to get sufficient thermal energy from laser source to convert into rGO, and therefore less electrical conductivity. The characterization performed on these samples showed that the optimized laser speed for electrode patterning was 2.5 mm s^{-1}, with a 100 μm rGO line width. Fig. 2g shows the variation of line width with the laser scan speed.

It can be noticed from Fig. 2h–k, at lower laser output powers, the patterning is not very clear, with the GO being probably only partially reduced (Fig. 2h). On the other hand, at very high laser powers, some of the scanned region gets ablated, leaving an enlarged and irregular micro-pattern (Fig. 2k). For higher laser powers, the rGO line width on GO film is neither constant nor uniform. The optimum laser power for the reduction of a 2.2 μm thick GO thin film was found to be 244 mW, with a complete and uniform reduction without disruption of the film. Fig. 2i presents the nearly linear variation of rGO line width with laser power for powers till 344 mW. At higher laser powers, the width increases abruptly due to the onset of the laser ablation process and the lateral heat dissipation from the illuminated region.

3.3 Electrical measurements: *I–V* measurement for laser patterned lines

The *I–V* curves presented in Fig. 3a show the variation of current with applied voltage through rGO lines obtained at different laser scan speeds. The resistance (or conductivity) values measured using two-point probes for 5 mm long laser-patterned lines are shown in Fig. 3b. These measurements indicate a linear dependence between the current and the voltage drop,

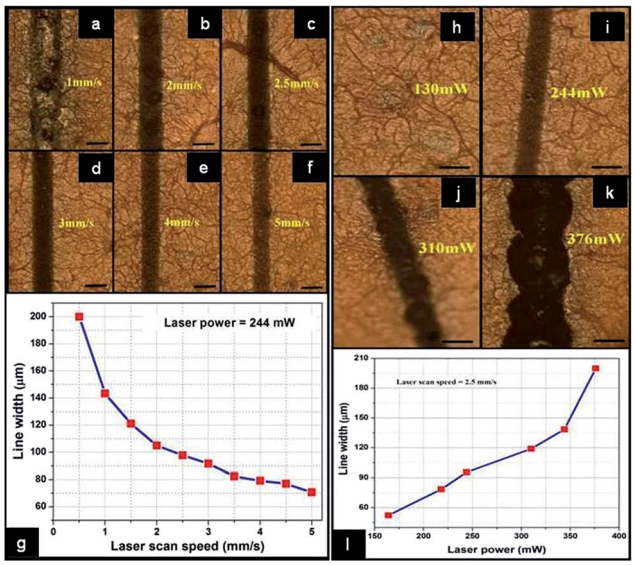

Fig. 2 Optimization of finger type electrode width on GO thin film by direct laser writing using various laser scan speed at constant laser power (244 mW): (a) 1.0 mm s^{-1}, (b) 2.0 mm s^{-1}, (c) 2.5 mm s^{-1}, (d) 3.0 mm s^{-1}, (e) 4.0 mm s^{-1} and (f) 5.0 mm s^{-1}; (g) graph showing the relation between direct laser scan speed and finger electrode width on GO thin film. Scale bars = 100 μm. Optimization of finger type electrode width on GO thin film by direct laser writing using various laser powers at constant laser scan speed (2.5 mm s^{-1}): (h) 130 mW, (i) 244 mW, (j) 310 mW and (k) 376 mW; (l) graph showing the relation between laser incident power and finger electrode width on GO thin film (scale bar = 100 μm).

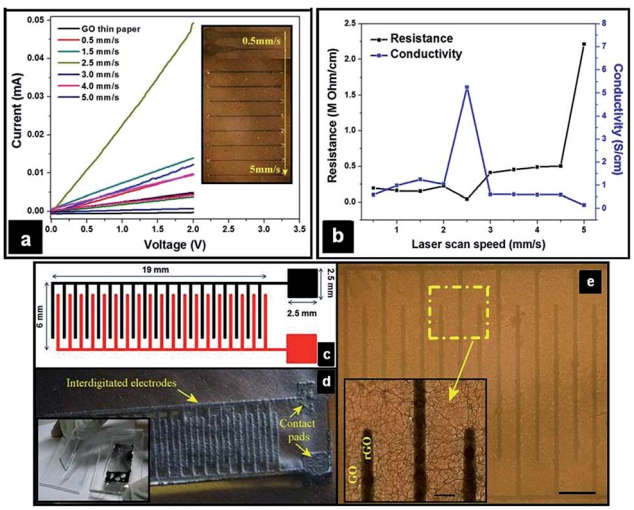

Fig. 3 Electrical conductivity measurement of finger electrodes on GO film for micro-supercapacitor device (a) *I–V* measurement of different finger line drawn on thin GO film at different laser scan speed (0.5 to 5.0 mm s^{-1}). (b) Relation between the electrical properties (resistance/conductivity) and the laser scan speeds for finger electrodes pattern on GO thin film. Schematic drawing (c) and optical image (d) of the micro-supercapacitor fabricated in this work. Inset shows the device inside glass cavity; (e) optical image of rGO and GO patterns on GO film for interdigitated electrode (scale bar = 1 mm). Inset presents a higher magnification image of the yellow square area (scale bar = 200 μm).

pointing the Ohmic behavior of the conducting rGO lines.[49] In contrast, the GO thin film shows nearly insulating behavior with high resistance (>5 × 10^6 Ω cm^{-1}). The conductivity of film increases gradually as the scan speed is decreased from the highest value (5.0 mm s^{-1}), reaching a local maxima at an optimized scan rate of 2.5 mm s^{-1}. This improvement of the GO reduction can be attributed to higher laser irradiation dose received by the sample resulting in higher local temperature and wider lines. Further decrease in the scan rate down to 1.5 mm s^{-1} results in a fast drop in the film conductivity probably due to increased overheating of sample and film damage due to ablation as clearly seen in Fig. 3a and b. Fig. 3b concludes that the scan rate must be carefully tuned in order to optimize the electrical parameters of the rGO film.

3.4 Micro-supercapacitor: interdigitated patterned electrode

Fig. 3c shows the schematic drawing and the optical image of an as-fabricated micro-supercapacitor on a free-standing film. The fabricated micro-supercapacitor device (Fig. 3d) has 19 mm long and 6 mm wide electrodes, with contact pad areas of 6.25 mm^2. The optimized laser parameters used are: power = 244 mW, scan speed = 2.5 mm s^{-1}, laser pulse frequency = 0.9 kHz and laser fluence (pulse energy per surface area) = 2.5 × 10^{-4} J mm^{-2}. The optical image in Fig. 3d shows that each finger like electrode has 5 mm length, with uniform linear reduction. The inset of Fig. 3d shows the optical image of micro-supercapacitor packed in glass cavity with open glass cover. The width and spacing between interdigitated electrodes are 100 and 400 μm, respectively (Fig. 3e).

Fig. 4a shows the SEM image of the rGO and unreduced GO film. The darker area in the left side corresponds to rGO (inset shows the wrinkles on the rGO surfaces), and the lighter area towards the right side to unmodified GO film. As the GO can be easily converted to rGO by laser irradiation, it enables rGO–GO–rGO micro pattern for micro-supercapacitor devices to be produced in a scalable and simple manner by laser-patterning of GO thin film.[50] The active rGO electrode material, formed using direct local laser heating, is apparently less uniform probably due to porosity that could be induced by the gases originated by the decomposition of the oxygenated functional groups (epoxy, hydroxyl, carboxyl and carbonyl groups) along with water vapor produced. For reduction of GO film through laser, the presence of oxygen amount (at%) has been measured by EDX for laser written electrodes on GO film with different laser speed and laser power. At 5.0, 4.0, 3.0, 2.5, 2.0 and 1.0 mm s^{-1} laser speed, the oxygen at% was 22.3, 17.7, 12.1, 8.9, 8.4, 7.9, respectively (at fixed laser P = 244 mW). The different laser power such as 130, 244, 310 and 376 mW shows the 33.4, 9.1, 8.3 and 7.2 at% of oxygen, respectively (at fixed s = 2.5 mm s^{-1}). The both observation confirms the more removal of oxygen containing functional groups at lower scan speed and higher laser power. The rGO has a negative thermal expansion coefficient, so local laser heating could make the treated area shrink, which in turn could lead to defects in the linear shaped graphene patterns on the GO film.[51] Fig. 4b shows the contact pad which was connected to Au wire with the help of silver paste.

Raman spectroscopy is a powerful tool for characterizing the structural properties of sp^2 carbon materials and can be helpful to reveal the quality of synthesized sample in terms of number of graphene layers, degree of defects and varying doping levels.[52] The Raman spectra of GO thin film and laser reduced GO as used for micro-supercapacitor are shown in Fig. 4c. The Raman spectrum of the GO and rGO shows two characteristic peaks near ~1351 and ~1595 cm^{-1} that correspond to the D and G bands, respectively.[53,54] The weak and broad peak around 2720 cm^{-1} corresponds to 2D band in GO and rGO samples.[50] The peak at 1351 cm^{-1} corresponds to the Raman-inactive A_{1g} in-plane breathing vibration mode, and is related to the defects and disorder present in graphitic layers. The G-band assigned to the Raman-active E_{2g} mode corresponds to the stretching vibration in the basal-plane of graphite, and is generally used to identify well-ordered materials.[55] The ratio between the intensities of D and G bands, I_D/I_G, is an important factor for evaluating the amount of structural defects present in graphitic materials.[56,57] The I_D/I_G ratio slightly increases for rGO from 0.89 to 0.92, which may be due to the creation of defects and porosity during laser induced thermal processing. This can also be attributed to a decrease in the size of reduced and patterned graphene domains and defects creation by gases escaped from the material during processing.[58] The Raman peak at 2950 cm^{-1} is associated with a D + G combination mode and is also induced by disorder.[57] The intensity of D + G band in rGO is higher than the GO which also confirms defective nature of rGO as compared to GO thin film.

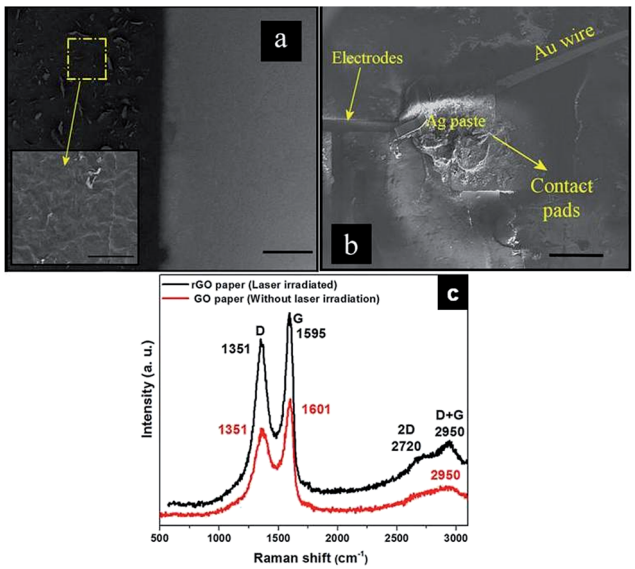

Fig. 4 SEM micrographs of: (a) rGO/GO interface (scale bar = 200 μm; inset scale bar = 10 μm) and (b) macro-contacts made using Au wire and Ag paste (scale bar = 1 mm). (c) Raman spectra of GO and rGO patterns used for the fabrication of micro-supercapacitor device.

3.5 Electrochemical performance

The interdigitated micro-supercapacitor was subjected to cyclic voltage sweeps at various scan rates without electrolyte (CI) and

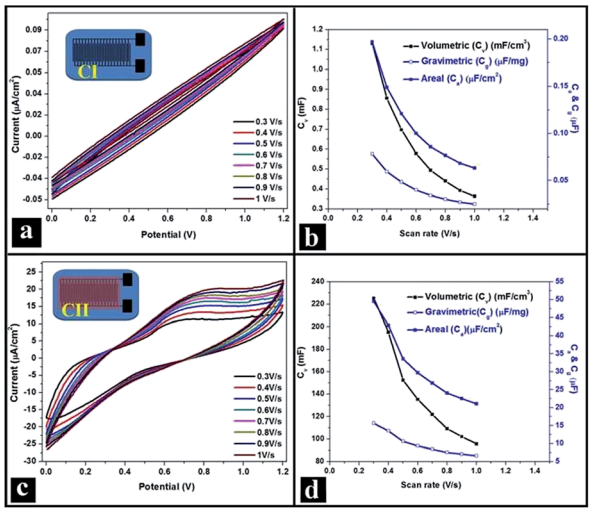

Fig. 5 CV and different capacitances with scan rates: (a) CV and (b) corresponding capacitances at different scan rate for as fabricated micro-supercapacitor without any additional electrolyte (CI); (c) CV and (d) corresponding capacitances at different scan rate for as fabricated micro-supercapacitor with 0.1 M Na_2SO_4 electrolyte (CII – electrolyte poured drop wise on surface of micro-supercapacitor device).

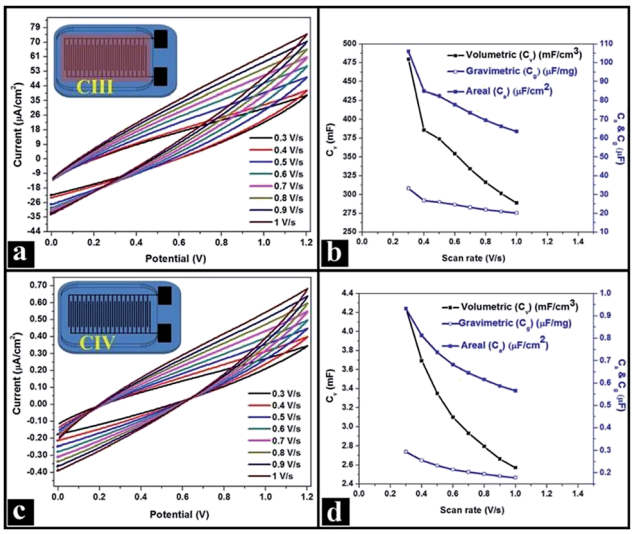

Fig. 6 CV and different capacitances with scan rates: (a) CV and (b) corresponding capacitances at different scan rate for as fabricated micro-supercapacitor with 0.1 M Na_2SO_4 electrolyte filled in glass cavity (CIII); (c) CV and (d) corresponding capacitances at different scan rate for as fabricated micro-supercapacitor after removing electrolyte from glass cavity (CIV).

in open air as shown in Fig. 5a. The gravimetric, areal and volumetric capacitances are plotted in Fig. 5b as a function of the scan rate, shows decreasing values as the scan rates get higher. The ions in the unreduced GO and free charges in reduced rGO contribute to the small values of capacitance, since no electrolyte is used. The rounding off of the voltamogram edges and the decrease in capacitance at high scan rates is due to the easy movement of ions already present in unreduced GO, between the interdigitated electrodes. The maximum values of capacitance for CI case, calculated at 0.3 V s^{-1} scan rate, are 0.078 μF mg^{-1}, 0.19 μF cm^{-2} and 1.12 mF cm^{-3} corresponding to gravimetric, areal and volumetric capacitance, respectively. After pouring a small amount of liquid electrolyte on the interdigitated micro-supercapacitor device (CII), its volumetric capacitance get increased by more than three orders of magnitude compared to CI. Fig. 5c and d represent the CV measurements in the electrolyte and the corresponding capacitances, respectively. In this case, the calculated values, at the same scan rates (0.3 V s^{-1}), are 15.6 μF mg^{-1}, 49.5 μF cm^{-2} and 225 mF cm^{-3} for gravimetric, areal and volumetric capacitances, respectively.

The above tests for CII were performed in open air at room temperature, in which the liquid electrolyte slowly evaporates and the concentration of electrolyte ions gets on increasing with time, affecting the performance of micro-supercapacitor and causing a distortion in the shape of the CV curves for longer measurement times. Thus, for longer term tests, the device was placed in a rectangular glass cavity with a lid (CIII) to prevent the evaporation of electrolyte and the as registered CV curves were shown in Fig. 6a. These measurements show larger area confined under the CV curves compared to results obtained in tests made without using glass cavity (CII). The values calculated at 0.3 V s^{-1} scan rate are 33.26 μF mg^{-1}, 106 μF cm^{-2} and 479 mF cm^{-3} for gravimetric, areal and volumetric capacitances, respectively (Fig. 6b). These capacitances are much more stable due to the non evaporation of liquid electrolyte during longer time measurements. Consequently, the concentration of ions in electrolyte is uniform during the CV measurements, and equal number of ions can move between the interdigitated electrodes.

The micro-supercapacitor fixed in a glass cavity was tested after complete drying of the electrolyte from the surface (glass cavity contains only micro-supercapacitor device – CIV) and we noticed that it shows much higher capacitance compared to the CI case (without electrolyte). The CV measurements and corresponding capacitances are shown in Fig. 6c and d, respectively. At 0.3 V s^{-1} scan rate, the measured gravimetric, areal and volumetric capacitances were 0.2 μF mg^{-1}, 0.9 μF cm^{-2} and 4.2 mF cm^{-3}, respectively. These values are higher as compared to CI (Fig. 5b) probably because some electrolyte ions were diffused inside the rGO finger electrode during the CIII CV measurements. The diffused ions inside the defective and porous structure thus enhanced the capacitance as measured in the CIV case. The comparisons of volumetric capacitances measured in different conditions are shown in Fig. 7.

Electrochemical Impedance Spectroscopy (EIS) is a very helpful technique for investigating electrical capacitance and obtaining complementary information about the electrical behavior of materials. The most extensively used plot for EIS analysis is the Nyquist plot. The plot represents the frequency responses of the electrode-electrolyte system for real (Z') and the imaginary ($-Z''$) components of the impedance. Fig. 8a shows the EIS graph obtained using 0.1 M Na_2SO_4 electrolyte solution in the frequency range from 0.1 mHz to 100 kHz with and ac-voltage amplitude of

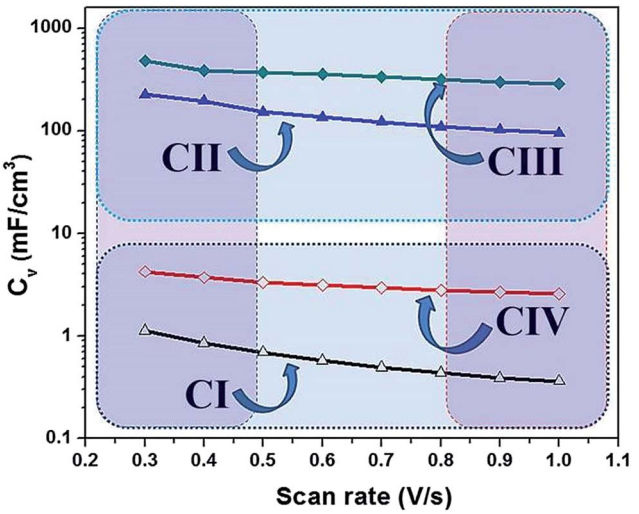

Fig. 7 Comparison of volumetric capacitances of as fabricated micro-supercapacitor in different conditions: CI – without any electrolyte, CII – with electrolyte, CIII – electrolyte filled in glass cavity and CIV – electrolyte removed from glass cavity.

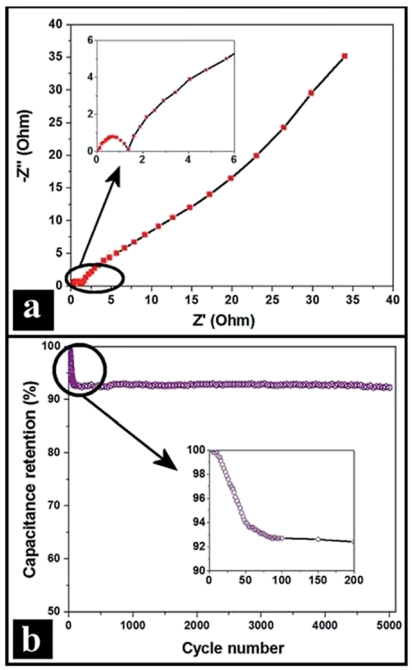

Fig. 8 (a) Nyquist plot and (b) long-term cycling stability of fabricated micro-supercapacitor device.

10 mV (CIII configuration). The intersection with the real axis at high-frequency regime represents the solution resistance and is related to the charge transfer between the electrode materials and electrolyte.[59,60] It is seen that the micro-supercapacitor shows very low solution resistance. The charge-transfer resistance (R_{ct}) can be measured from the diameter of the semi-circle region near the real axis (inset of Fig. 8a).[59–61] Here, the semi-circle appearing at the high frequency region has very low diameter, indicating a low charge-transfer resistance of ~1.4 Ω.

Numerous cycles are to be measured to assess the stability of the supercapacitor electrodes. The cycling stabilities of micro-supercapacitor devices were measured by using CV technique at a constant scan rate of 0.6 V s^{-1}. To calculate the cyclic stabilities of as fabricated micro-supercapacitor, up to 5000 consecutive CV cycles were performed, as shown in Fig. 8b. The specific capacitance retention of micro-supercapacitor is stable for over 5000 cycle. It remains stable near 92.5% of its maximum value from ~65 cycles to the end of testing at 5000 cycles, suggesting excellent stability. The linear interdigitated electrode with GO–rGO–GO structure was found to exhibit good cyclic stability, compared to the existing thin film super-capacitors.[43] The long cycling stability indicates that the fabricated rGO interdigitated electrodes help the ion transfer inside the rGO and GO interfaces. It is important to emphasize that a good cyclic stability for such devices is the main attribute needed for practical applications.

4. Conclusions

In this work we present a fabrication method that provides the transfer-free fabrication of linear graphene patterns on insulating GO thin film with high conductivity (5.2 S cm^{-1}). The as-fabricated micro-supercapacitors were tested with/without the presence of liquid electrolyte and in closed/open atmosphere for investigating their capacitive behaviour. The volumetric capacitance values of these devices increases significantly in the presence of the electrolyte when compared with bare measurements (no electrolyte), as expected. The micro-supercapacitor shows excellent stability without distortion and degradation even after 5000 cycles and a retention capacitance of 92.5%, which also indicates excellent stability. Considering the high simplicity, flexibility, and reliability in producing graphene patterns, the direct laser writing method can open a door for fabricating graphene pattern having a variety of sizes and shapes for advanced graphene-based devices. Also, these results indicate that this scalable and facile fabrication technique proves to be promising for application in integrated energy storage solid-state flexible micro-devices fabrication.

Acknowledgements

R. Kumar, R. Savu, A. R. Vaz, E. Joanni and S. A. Moshkalev would like to acknowledge CNPq and FAPESP (Brazil) for financial support.

Notes and references

1 B. Xu, S. Yue, Z. Sui, X. Zhang, S. Hou, G. Cao and Y. Yang, *Energy Environ. Sci.*, 2011, **4**, 2826–2830.
2 D. Kondo, K. Yagi, M. Sato, M. Nihei, Y. Awano, S. Sato and N. Yokoyama, *Chem. Phys. Lett.*, 2011, **514**, 294–300.
3 R. Kumar, R. K. Singh, P. K. Dubey, D. P. Singh, R. M. Yadav and R. S. Tiwari, *Adv. Mater. Interfaces*, 2015, **2**, 1500191.
4 M. Winter and R. J. Brodd, *Chem. Rev.*, 2004, **104**, 4245–4270.
5 G. Zhou, F. Li and H.-M. Cheng, *Energy Environ. Sci.*, 2014, **7**, 1307–1338.

6 R. Ye, Z. Peng, T. Wang, Y. Xu, J. Zhang, Y. Li, L. G. Nilewski, J. Lin and J. M. Tour, *ACS Nano*, 2015, **9**, 9244–9251.
7 R. Kumar, H.-J. Kim, S. Park, A. Srivastava and I.-K. Oh, *Carbon*, 2014, **79**, 192–202.
8 Y. Zhang, L. Gomez, F. N. Ishikawa, A. Madaria, K. Ryu, C. Wang, A. Badmaev and C. Zhou, *J. Phys. Chem. Lett.*, 2010, **1**, 3101–3107.
9 R. Kumar, R. K. Singh, P. Kumar Dubey, D. P. Singh, R. M. Yadav and R. S. Tiwari, *RSC Adv.*, 2015, **5**, 7112–7120.
10 R. Kumar, R. K. Singh, P. K. Dubey, D. P. Singh and R. M. Yadav, *ACS Appl. Mater. Interfaces*, 2015, **7**, 15042–15051.
11 R. Kumar, R. K. Singh, A. R. Vaz and S. A. Moshkalev, *RSC Adv.*, 2015, **5**, 67988–67995.
12 R. Kumar, R. K. Singh, R. Savu, P. K. Dubey, P. Kumar and S. A. Moshkalev, *RSC Adv.*, 2016, **6**, 26612–26620.
13 X. Wang and G. Shi, *Energy Environ. Sci.*, 2015, **8**, 790–823.
14 C. Hu, L. Song, Z. Zhang, N. Chen, Z. Feng and L. Qu, *Energy Environ. Sci.*, 2015, **8**, 31–54.
15 L. Li, Z. Wu, S. Yuan and X.-B. Zhang, *Energy Environ. Sci.*, 2014, **7**, 2101–2122.
16 L. Hu and Y. Cui, *Energy Environ. Sci.*, 2012, **5**, 6423–6435.
17 S. Park, M. Vosguerichian and Z. Bao, *Nanoscale*, 2013, **5**, 1727–1752.
18 Y. He, W. Chen, C. Gao, J. Zhou, X. Li and E. Xie, *Nanoscale*, 2013, **5**, 8799–8820.
19 M. F. El-Kady and R. B. Kaner, *ACS Nano*, 2014, **8**, 8725–8729.
20 R. S. Singh, V. Nalla, W. Chen, A. T. S. Wee and W. Ji, *ACS Nano*, 2011, **5**, 5969–5975.
21 Y. Shao, M. F. El-Kady, L. J. Wang, Q. Zhang, Y. Li, H. Wang, M. F. Mousavi and R. B. Kaner, *Chem. Soc. Rev.*, 2015, **44**, 3639–3665.
22 S. Chen, W. Ma, Y. Cheng, Z. Weng, B. Sun, L. Wang, W. Chen, F. Li, M. Zhu and H.-M. Cheng, *Nano Energy*, 2015, **15**, 642–653.
23 X. Peng, L. Peng, C. Wu and Y. Xie, *Chem. Soc. Rev.*, 2014, **43**, 3303–3323.
24 S. H. Lee, C. K. Jeong, G.-T. Hwang and K. J. Lee, *Nano Energy*, 2015, **14**, 111–125.
25 A. Ramadoss, B. Saravanakumar and S. J. Kim, *Nano Energy*, 2015, **15**, 587–597.
26 J. Lin, Z. Peng, Y. Liu, F. Ruiz-Zepeda, R. Ye, E. L. G. Samuel, M. J. Yacaman, B. I. Yakobson and J. M. Tour, *Nat. Commun.*, 2014, **5**, 5714.
27 Z. Peng, J. Lin, R. Ye, E. L. G. Samuel and J. M. Tour, *ACS Appl. Mater. Interfaces*, 2015, **7**, 3414–3419.
28 Y.-L. Zhang, Q.-D. Chen, H. Xia and H.-B. Sun, *Nano Today*, 2010, **5**, 435–448.
29 Y. Zhang, L. Guo, S. Wei, Y. He, H. Xia, Q. Chen, H.-B. Sun and F.-S. Xiao, *Nano Today*, 2010, **5**, 15–20.
30 S. Kawata, H.-B. Sun, T. Tanaka and K. Takada, *Nature*, 2001, **412**, 697–698.
31 X.-Z. Dong, Z.-S. Zhao and X.-M. Duan, *Appl. Phys. Lett.*, 2007, **91**, 124103.
32 D.-Y. Yang, S. H. Park, T. W. Lim, H.-J. Kong, S. W. Yi, H. K. Yang and K.-S. Lee, *Appl. Phys. Lett.*, 2007, **90**, 013113.
33 S. Wang, B. Hsia, C. Carraro and R. Maboudian, *J. Mater. Chem. A*, 2014, **2**, 7997–8002.
34 J. Chmiola, C. Largeot, P.-L. Taberna, P. Simon and Y. Gogotsi, *Science*, 2010, **328**, 480–483.
35 D. Pech, M. Brunet, P.-L. Taberna, P. Simon, N. Fabre, F. Mesnilgrente, V. Conédéra and H. Durou, *J. Power Sources*, 2010, **195**, 1266–1269.
36 D. Pech, M. Brunet, H. Durou, P. Huang, V. Mochalin, Y. Gogotsi, P.-L. Taberna and P. Simon, *Nat. Nanotechnol.*, 2010, **5**, 651–654.
37 M. D. Stoller, S. Park, Y. Zhu, J. An and R. S. Ruoff, *Nano Lett.*, 2008, **8**, 3498–3502.
38 A. A. Balandin, S. Ghosh, W. Bao, I. Calizo, D. Teweldebrhan, F. Miao and C. N. Lau, *Nano Lett.*, 2008, **8**, 902–907.
39 K. I. Bolotin, K. J. Sikes, Z. Jiang, M. Klima, G. Fudenberg, J. Hone, P. Kim and H. L. Stormer, *Solid State Commun.*, 2008, **146**, 351–355.
40 J.-U. Lee, D. Yoon and H. Cheong, *Nano Lett.*, 2012, **12**, 4444–4448.
41 M. F. El-Kady and R. B. Kaner, *Nat. Commun.*, 2013, **4**, 1475.
42 M. F. El-Kady, V. Strong, S. Dubin and R. B. Kaner, *Science*, 2012, **335**, 1326–1330.
43 W. Gao, N. Singh, L. Song, Z. Liu, A. L. M. Reddy, L. Ci, R. Vajtai, Q. Zhang, B. Wei and P. M. Ajayan, *Nat. Nanotechnol.*, 2011, **6**, 496–500.
44 Z. S. Wu, K. Parvez, X. Feng and K. Müllen, *Nat. Commun.*, 2013, **4**, 2487.
45 W. S. Hummers and R. E. Offeman, *J. Am. Chem. Soc.*, 1958, **80**, 1339–1339.
46 D. R. Dreyer, S. Park, C. W. Bielawski and R. S. Ruoff, *Chem. Soc. Rev.*, 2010, **39**, 228–240.
47 K. R. Koch, *J. Chem. Educ.*, 1982, **59**, 973.
48 Y. Gogotsi and P. Simon, *Science*, 2011, **334**, 917–918.
49 Y. Tao, B. Varghese, M. Jaiswal, S. Wang, Z. Zhang, B. Oezyilmaz, K. P. Loh, E. S. Tok and C. H. Sow, *Appl. Phys. A: Mater. Sci. Process.*, 2011, **106**, 523–531.
50 H. Fatt Teoh, Y. Tao, E. Soon Tok, G. Wei Ho and C. Haur Sow, *J. Appl. Phys.*, 2012, **112**, 064309.
51 D. Yoon, Y.-W. Son and H. Cheong, *Nano Lett.*, 2011, **11**, 3227–3231.
52 Y. Zhu, S. Murali, W. Cai, X. Li, J. W. Suk, J. R. Potts and R. S. Ruoff, *Adv. Mater.*, 2010, **22**, 3906–3924.
53 C.-h. Huang, R.-a. Doong, D. Gu and D. Zhao, *Carbon*, 2011, **49**, 3055–3064.
54 W. Gao, Y. Wan, Y. Dou and D. Zhao, *Adv. Energy Mater.*, 2011, **1**, 115–123.
55 M. Deng, X. Yang, M. Silke, W. Qiu, M. Xu, G. Borghs and H. Chen, *Sens. Actuators, B*, 2011, **158**, 176–184.
56 A. C. Ferrari, *Solid State Commun.*, 2007, **143**, 47–57.
57 M. A. Pimenta, G. Dresselhaus, M. S. Dresselhaus, L. G. Cancado, A. Jorio and R. Saito, *Phys. Chem. Chem. Phys.*, 2007, **9**, 1276–1290.
58 F. Tuinstra and J. L. Koenig, *J. Chem. Phys.*, 1970, **53**, 1126–1130.
59 Y. Zhu, Z. Wu, M. Jing, H. Hou, Y. Yang, Y. Zhang, X. Yang, W. Song, X. Jia and X. Ji, *J. Mater. Chem. A*, 2015, **3**, 866–877.
60 Y. Wang, Z. Shi, Y. Huang, Y. Ma, C. Wang, M. Chen and Y. Chen, *J. Phys. Chem. C*, 2009, **113**, 13103–13107.
61 S. Saha, M. Jana, P. Samanta, N. Chandra Murmu, N. H. Kim, T. Kuila and J. H. Lee, *RSC Adv.*, 2014, **4**, 44777–44785.

